Hierarchical Assembly and Modeling of DNA Nanotube Networks Using Y-Shaped DNA Origami Seeds

Yanqi Jiang[a,*], Michael S. Pacella[a,*], Sojeong Lee[b], Jasen Zhang[a], Jonathan A. Gunn[a], Paul Vallejo[a], Pragya Singh[a], Tiffany Hou[a], Evan Liu[a] and Rebecca Schulman[a,c]

[a]Department of Chemical and Biomolecular Engineering, Johns Hopkins University, Baltimore, Maryland 21218, United States

[b]Department of Biomedical Engineering, Johns Hopkins University, Baltimore, Maryland 21218, United States

[c]Department of Computer Science, Johns Hopkins University, Baltimore, Maryland 21218, United States

* These authors contributed equally.

Contents

1. **DNA Nanotube and Seed Design with Sequences**
   - 1.1 Design of DNA nanotubes
   - 1.2 Design of Y-shaped DNA origami seeds
   - 1.3 Design of labeling strands and attachments

2. **Methods and Protocols**
   - 2.1 Self-assembly of nanotube networks
     - 2.1.1 Y-shaped DNA origami seeds (YSA and YSB)
     - 2.1.2 Y-seeded nanotube architecture (YNA and YNB) growth
     - 2.1.3 Network formation
   - 2.2 Microscopy and Processing

3. **Additional Data and Analysis**
   - 3.1 Network growth simulation
   - 3.2 Edge and blob detection

4. **Supplementary Figures**

1. DNA Nanotube and Seed Design with Sequences

All DNA strands used in this study were synthesized by Integrated DNA Technologies, Inc. (IDT) except the M13mp18 scaffold strand, which was purchased from Bayou Biolabs. The DNA nanotube tile and adapter strands were PAGE purified while Cy3 and ATTO488 fluorophore-modified strands and biotin-modified strands were HPLC purified. Concentrations for DNA tile and adapter strands were determined by measuring absorbance at 260 nm [1]; for other strands we relied on IDT to determine solution concentrations.

1.1. Design of DNA nanotubes

The tile design and sequences in this study are adopted from Rothemund et al. [2] Nanotubes contained two types of DNA tiles, termed REd and SEd arranged in a diagonal lattice (Figure S1), and the sequences for REd and SEd tiles are listed in the Table S1 below.

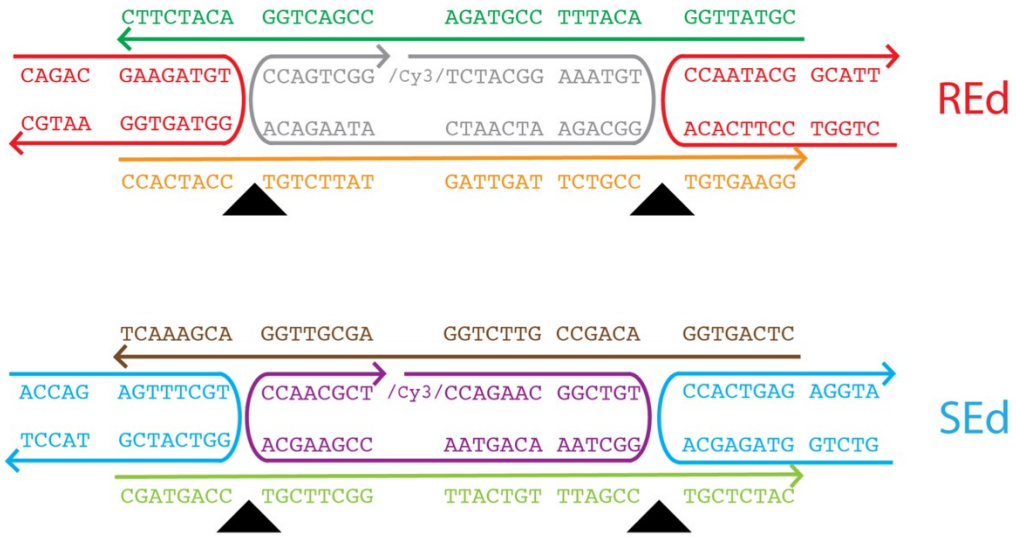

Figure S1: Design schematic of DAE-E DNA tiles used to form nanotubes. The two types of tiles assemble into a diagonal lattice that forms a nanotube. [2]

Table S1: REd and SEd nanotube tile sequences: (5'--> 3')

RE-1	CGTATTGGACATTTCCGTAGACCGACTGGACATCTTC
RE-2EE01	CTGGTCCTTCACACCAATACGGCATT
RE-3Cy3	/Cy3/TCTACGGAAATGTGGCAGAATCAATCATAAGACACCAGTCGG
RE-4	CAGACGAAGATGTGGTAGTGGAATGC
RE-5	CCACTACCTGTCTTATGATTGATTCTGCCTGTGAAGG
SE-1	CTCAGTGGACAGCCGTTCTGGAGCGTTGGACGAAACT

SE-2DIAG	GTCTGGTAGAGCACCACTGAGAGGTA
SE-3Cy3	/Cy3/CCAGAACGGCTGTGGCTAAACAGTAACCGAAGCACCAACGCT
SE-4DIAG	ACCAGAGTTTCGTGGTCATCGTACCT
SE-5	CGATGACCTGCTTCGGTTACTGTTTAGCCTGCTCTAC

/Cy3/ denotes Cy3 fluorophore covalently attached to the 5' end of the DNA.

1.2. Design of Y-shaped DNA origami seeds

The DNA origami seeds used in this study are Y-shaped DNA origami nanostructures. YSA is directly adopted from Jorgenson et al.[3] and we revised its design to build YSB. YSA and YSB only have different sets of adapter tiles, allowing each of them to nucleate nanotubes from their 3 arms.

Staples and struts design

The staples and struts design for the Y-seeds in this study are adopted from Jorgenson et al.[3] Both YSA and YSB used the same staples and struts.

Adapter strands design

The adapter tiles were designed to serve as templates onto which nanotube tiles can attach. The complete tile sequences of the YSA adapters are shown below (Supplementary Figure S2 and Table S2-4). The YSB adapters consisted of the YSA strands whose names in the lists that follow end in 1_YSA, 3_YSA, or 5_YSA (the orange, green and brown strands in Supplementary Figure S2) but have different strands that present sticky ends (those in blue in Supplementary Figure S2 and with names ending in 2_YSA or 2_YSB). The sequences that are different in YSA and YSB are in red type in Table S2-4; the corresponding sequences for the YSB adapters are then listed in Table S5. For example, the strand AD1_2REd_armC_2_YSA is replaced by AD1_2REd_armC_2_YSB when making YSB.

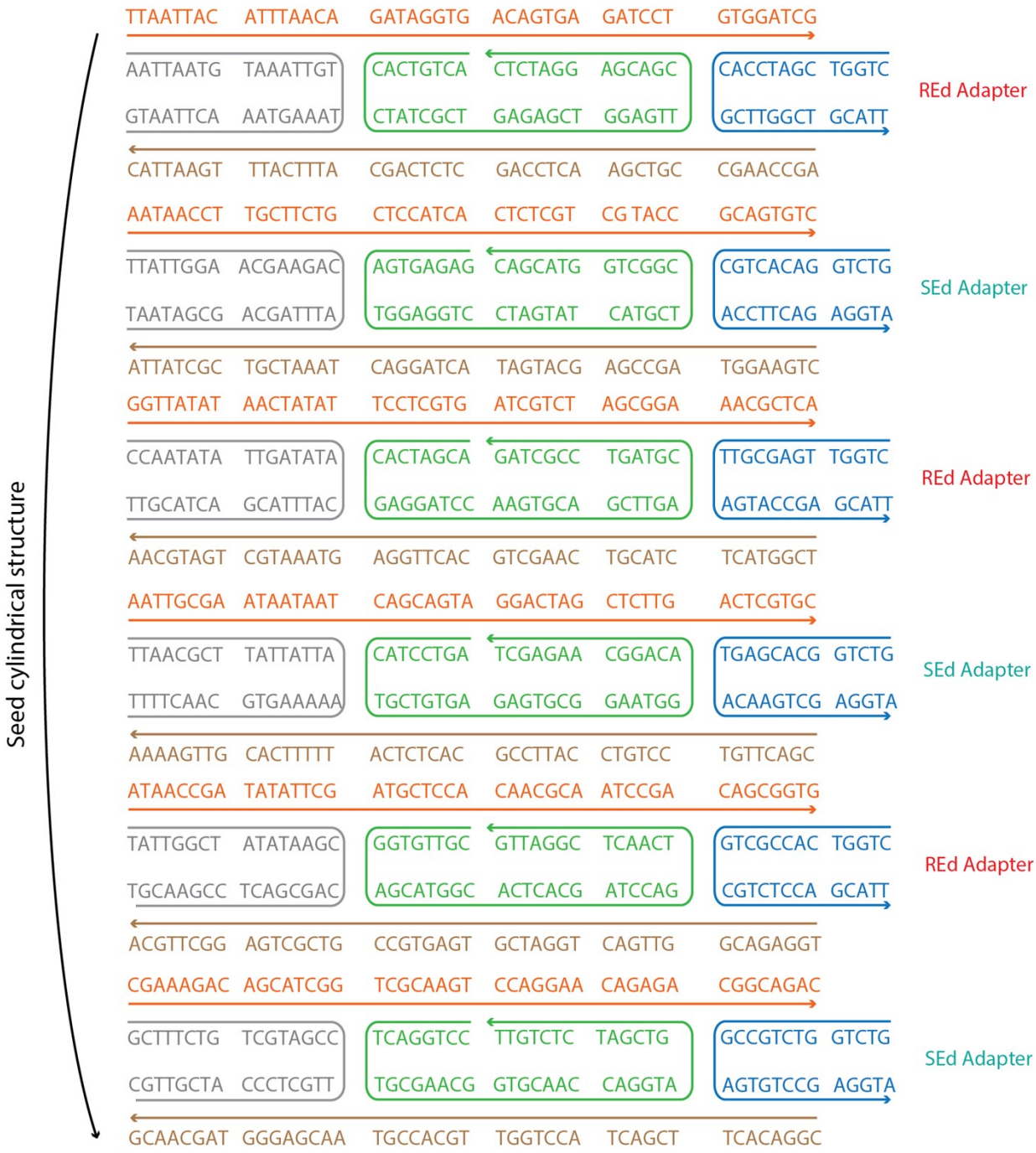

Figure S2: The structure of YSA adapters for arm A of the Y-shaped seed. The adapters on each of the three arms share the depicted structure of adapters with different sequences). The gray lines and corresponding sequences are parts of the M13mp18 scaffold.

Table S2: YSA A-Arm Adapter Tile Sequences

AD1REd_armA_1_YSA	TTA ATT ACA TTT AAC AGA TAG GTG ACA GTG AGA TCC TGT GGA TCG
AD1_2REd_armA_3_YSA	ACT GTC ACC TAT CGC TGA GAG CTG GAG TTC GAC GAG GAT CTC
AD2REd_armA_5_YSA	AGC CAA GCC GTC GAA CTC CAG CTC TCA GCA TTT CAT TTG AAT TAC
AD1_2REd_armA_2_YSA	CTG GTC GAT CCA CGC TTG GCT GCA TT
AD3SEd_armA_1_YSA	AAT AAC CTT GCT TCT GCT CCA TCA CTC TCG TCG TAC CGC AGT GTC
AD3_4SEd_armA_3_YSA	GAG AGT GAT GGA GGT CCT AGT ATC ATG CTC GGC TGG TAC GAC
AD4SEd_armA_5_YSA	CTG AAG GTA GCC GAG CAT GAT ACT AGG ACT AAA TCG TCG CTA TTA
AD3_4SEd_armA_2_YSA	GTC TGG ACA CTG CAC CTT CAG AGG TA
AD5REd_armA_1_YSA	GGT TAT ATA ACT ATA TTC CTC GTG ATC GTC TAG CGG AAA CGC TCA
AD5_6REd_armA_3_YSA	ACG ATC ACG AGG ATC CAA GTG CAG CTT GAC GTA GTC CGC TAG
AD6REd_armA_5_YSA	TCG GTA CTC TAC GTC AAG CTG CAC TTG GAG TAA ATG CTG ATG CAA
AD5_6REd_armA_2_YSA	CTG GTT GAG CGT TAG TAC CGA GCA TT
AD7SEd_armA_1_YSA	AAT TGC GAA TAA TAA TCA GCA GTA GGA CTA GCT CTT GAC TCG TGC
AD7_8SEd_armA_3_YSA	AGT CCT ACT GCT GTG AGA GTG CGG AAT GGA CAG GCA AGA GCT
AD8SEd_armA_5_YSA	CGA CTT GTC CTG TCC ATT CCG CAC TCT CAT TTT TCA CGT TGA AAA
AD7_8SEd_armA_2_YSA	GTC TGG CAC GAG TAC AAG TCG AGG TA
AD9REd_armA_1_YSA	ATA ACC GAT ATA TTC GAT GCT CCA CAA CGC AAT CCG ACA GCG GTG
AD9_10REd_armA_3_YSA	CGT TGT GGA GCA TGG CAC TCA CGA TCC AGT CAA CTC GGA TTG
AD10REd_armA_5_YSA	TGG AGA CGG TTG ACT GGA TCG TGA GTG CCG TCG CTG AGG CTT GCA
AD9_10REd_armA_2_YSA	CTG GTC ACC GCT GCG TCT CCA GCA TT
AD11SEd_armA_1_YSA	CGA AAG ACA GCA TCG GTC GCA AGT CCA GGA ACA GAG ACG GCA GAC
AD11_12SEd_armA_3_YSA	CCT GGA CTT GCG AAC GGT GCA ACC AGG TAG TCG ATC TCT GTT
AD12SEd_armA_5_YSA	CGG ACA CTT CGA CTA CCT GGT TGC ACC GTA ACG AGG GTA GCA ACG
AD11_12SEd_armA_2_YSA	GTC TGG TCT GCC GAG TGT CCG AGG TA

Table S3: YSA B-arm Adapter Tile Sequences

AD1REd_armB_1_YSA	ACA ACA TGT TCA GCT ACC AGC ACG ACT CTA GGT GTA GCG TGA GCG
AD1_2REd_armB_3_YSA	AGA GTC GTG CTG GCG TCC GAG ACC TCA CAG GTG ACT ACA CCT
AD2REd_armB_3_YSA	AGC GAG GAT CAC CTG TGA GGT CTC GGA CGA TGC AGA ACG CGC CTG
AD1_2REd_armB_2_YSA	CTG GTC GCT CAC GTC CTC GCT GCA TT
AD3SEd_armB_1_YSA	CGC ACT CAT CGA GAA CCG ATC CGA CGC CAT GTC CAA GAC GGA ACA
AD3_4SEd_armB_3_YSA	TGG CGT CGG ATC GCT ACC AGT CAC ACC ACT AGC ACT TGG ACA

AD4SEd_armB_3_YSA	GAC TCG GCT GCT AGT GGT GTG ACT GGT AGA AGC AAG CCG TTT TTA
AD3_4SEd_armB_2_YSA	GTC TGT GTT CCG TGC CGA GTC AGG TA
AD5REd_armB_1_YSA	AAT AAG AGC AAG AAA CCT GGA CGA GCT ACC AAG ACC ATT CCT GAC
AD5_6REd_armB_3_YSA	GTA GCT CGT CCA GAG GCT GCG TTC GTC GGT AGT GTG GTC TTG
AD6REd_armB_3_YSA	CAC TCA GGC ACT ACC GAC GAA CGC AGC CTA ATG AAA TAG CAA TAG
AD5_6REd_armB_2_YSA	CTG GTG TCA GGA ACC TGA GTG GCA TT
AD7SEd_armB_1_YSA	GCA GTA TGT TAG CAA ATG GAG CGA ACC GTC ATG CCT GTT GCT CGC
AD7_8SEd_armB_3_YSA	ACG GTT CGC TCC AAC ATC GTC ACA GTG GCT ACG GCA GGC ATG
AD8SEd_armB_3_YSA	GTA TCC GAC CGT AGC CAC TGT GAC GAT GTC GTA GAA AAT ACA TAC
AD7_8SEd_armB_2_YSA	GTC TGG CGA GCA ATC GGA TAC AGG TA
AD9REd_armB_1_YSA	TCA GAG CCG CCA CCC TGT GTC CTG CTC CTA GTC GCA GAT GCG GAG
AD9_10REd_armB_3_YSA	AGG AGC AGG ACA CGA GCC AGC GTA AGG ATG TCG GCT GCG ACT
AD10REd_armB_3_YSA	AGT CCA CAC CGA CAT CCT TAC GCT GGC TCC AGA ACC GCC ACC CTC
AD9_10REd_armB_2_YSA	CTG GTC TCC GCA TTG TGG ACT GCA TT
AD11SEd_armB_1_YSA	AAT GGA AAG CGC AGT CGT AGA CCT AGA GGC GAC GCA AGT GTC TCG
AD11_12SEd_armB_3_YSA	CCT CTA GGT CTA CCG TGG TTC GGA GCT GAT CGA GTT GCG TCG
AD12SEd_armB_3_YSA	CGC CAA TCC TCG ATC AGC TCC GAA CCA CGT CTG AAT TTA CCG TTC
AD11_12SEd_armB_2_YSA	GTC TGC GAG ACA CGA TTG GCG AGG TA

Table S4: YSA C-arm Adapter Tile Sequences

AD1REd_armC_1_YSA	GTA ATC TTG ACA AGA AGT CTC GGT TGG ACA AGG CGA CTG GAG TGA
AD1_2REd_armC_3_YSA	GTC CAA CCG AGA CAG CGT TAC GAG GTA CAG TCA GGT CGC CTT
AD2REd_armC_3_YSA	TAA TGG CAC TGA CTG TAC CTC GTA ACG CTC CGG ATA TTC ATT ACC
AD1_2REd_armC_2_YSA	CTG GTT CAC TCC ATG CCA TTA GCA TT
AD3SEd_armC_1_YSA	GAA TCG TCA TAA ATA TGC CTA GAC TCC GAC GTG GAA CGC TAA CCA
AD3_4SEd_armC_3_YSA	TCG GAG TCT AGG CTG GCA TGA GCA TCT CGC AGT GGT TCC ACG
AD4SEd_armC_3_YSA	CTG GAA GTC ACT GCG AGA TGC TCA TGC CAT CAT TGA ATC CCC CTC
AD3_4SEd_armC_2_YSA	GTC TGT GGT TAG CAC TTC CAG AGG TA
AD5REd_armC_1_YSA	AAT ATC GCG TTT TAA TAG CGG AGG TAC GGA GTC ACC ATT GCC ATG
AD5_6REd_armC_3_YSA	CCG TAC CTC CGC TTC GCA TCT GAG TCG CTG GAT GTG GTG ACT
AD6REd_armC_3_YSA	TGA ACC AGC ATC CAG CGA CTC AGA TGC GAT CGA GCT TCA AAG CGA
AD5_6REd_armC_2_YSA	CTG GTC ATG GCA ACT GGT TCA GCA TT
AD7SEd_armC_1_YSA	TTT TAA ATA TGC AAC TGA CTC TCG ACA TGG TCC GAA CTC GCT TGA

AD7_8SEd_armC_3_YSA	CAT GTC GAG AGT CAC GCT CTA CTA CGC CAT CGG TGT TCG GAC
AD8SEd_armC_3_YSA	TGA GGC TAA CCG ATG GCG TAG TAG AGC GTA AAG TAC GGT GTC TGG
AD7_8SEd_armC_2_YSA	GTC TGT CAA GCG ATA GCC TCA AGG TA
AD9REd_armC_1_YSA	AAG GTG GCA TCA ATT CGT GCC TTC ACG TTG CTG TCG TTC CTA TCG
AD9_10REd_armC_3_YSA	AAC GTG AAG GCA CAG ACA CTC CGT CAG AGG CAA CAC GAC AGC
AD10REd_armC_3_YSA	CAT GAG GCG TTG CCT CTG ACG GAG TGT CTT ACT AAT AGT AGT AGC
AD9_10REd_armC_2_YSA	CTG GTC GAT AGG AGC CTC ATG GCA TT
AD11SEd_armC_1_YSA	AAA ATT AAG CAA TAA ACG ACG GAC GCT TGT GGA TGA GGT CGC ACT
AD11_12SEd_armC_3_YSA	CAA GCG TCC GTC GAG ACA GTG TAG GAC GAC ACA GCT CAT CCA
AD12SEd_armC_3_YSA	GGC TCG CTC TGT GTC GTC CTA CAC TGT CTG CCT CAG AGC ATA AAG
AD11_12SEd_armC_2_YSA	GTC TGA GTG CGA CAG CGA GCC AGG TA

Table S5: YSB Adapter A/B/C-arm Tile Sequences (Strand 2)

AD1_2REd_armA_2_YSB	CAG ACC GAT CCA CGC TTG GCT AAT GC
AD3_4SEd_armA_2_YSB	ACC AGG ACA CTG CAC CTT CAG TAC CT
AD5_6REd_armA_2_YSB	CAG ACT GAG CGT TAG TAC CGA AAT GC
AD7_8SEd_armA_2_YSB	ACC AGG CAC GAG TAC AAG TCG TAC CT
AD9_10REd_armA_2_YSB	CAG ACC ACC GCT GCG TCT CCA AAT GC
AD11_12SEd_armA_2_YSB	ACC AGG TCT GCC GAG TGT CCG TAC CT
AD1_2REd_armB_2_YSB	CAG ACC GCT CAC GTC CTC GCT AAT GC
AD3_4SEd_armB_2_YSB	ACC AGT GTT CCG TGC CGA GTC TAC CT
AD5_6REd_armB_2_YSB	CAG ACG TCA GGA ACC TGA GTG AAT GC
AD7_8SEd_armB_2_YSB	ACC AGG CGA GCA ATC GGA TAC TAC CT
AD9_10REd_armB_2_YSB	CAG ACC TCC GCA TTG TGG ACT AAT GC
AD11_12SEd_armB_2_YSB	ACC AGC GAG ACA CGA TTG GCG TAC CT
AD1_2REd_armC_2_YSB	CAG ACT CAC TCC ATG CCA TTA AAT GC
AD3_4SEd_armC_2_YSB	ACC AGT GGT TAG CAC TTC CAG TAC CT
AD5_6REd_armC_2_YSB	CAG ACC ATG GCA ACT GGT TCA AAT GC
AD7_8SEd_armC_2_YSB	ACC AGT CAA GCG ATA GCC TCA TAC CT
AD9_10REd_armC_2_YSB	CAG ACC GAT AGG AGC CTC ATG AAT GC
AD11_12SEd_armC_2_YSB	ACC AGA GTG CGA CAG CGA GCC TAC CT

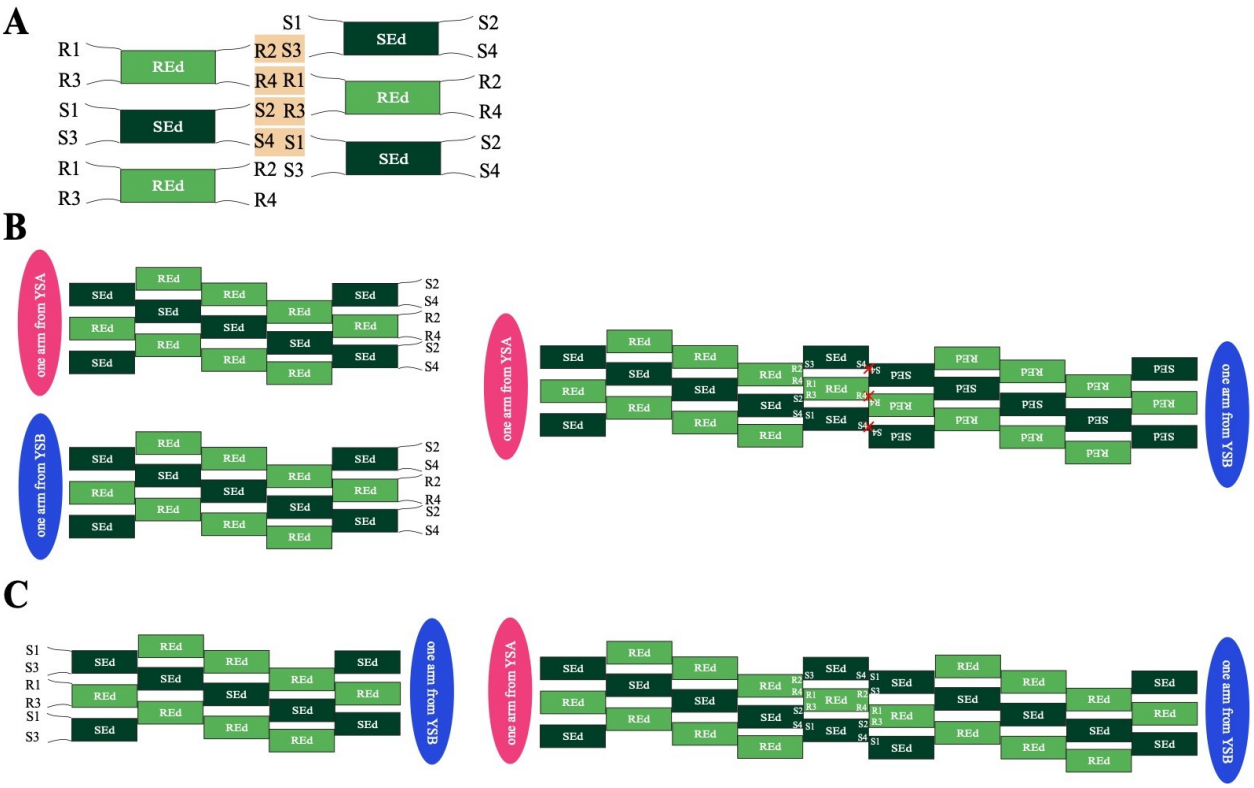

Figure S3: The design of different adapters for YSA and YSB to ensure complementary ends of YNA and YNB. (A) Shows the simplified diagram of REd and SEd tile assembly according to Figure S1 and the hybridization of their adapter strands. R1,2,3,4 and S1,2,3,4 denote the four sticky ends of REd and SEd, which assemble diagonally, allowing hybridization only between specific pairs of strands (e.g. R2-S3, R4-R1, etc.) (B) If YSA and YSB used the same adapter (that is, if YSA were entirely identical to YSB), the YNA and YNB sticky ends would be identical and would not bind to one another, as the diagram on the right side shows. (C) By changing the adapter design of YSB so that the nanotubes are able to nucleate on the other side of the origami structure, we ensure that YNB will have complementary sticky ends to YNA, and end-to-end joining will occur specifically between YNA and YNB. Connections between YNA-YNA or YNB-YNB cannot form due to their identical sticky ends.

1.3 Design of labeling strands and attachments

The design of the fluorescent labelling strands for nanotube seeds was adopted from Jorgenson et al [3]. As mentioned in the text, some experiments used ATTO 647 to label YSA and ATTO 488 fluorophore to label YSB while in other experiments ATTO 488 was used to label both YSA and YSB. To label each of these structures, we used a labelling system consisting of 80 attachment strands and a labeling strand. Each attachment strand contains one domain that binds to the unfolded portion of M13mp18 scaffold and the other domain that binds to the labeling strand. The labeling strand has a fluorophore dye on its 5' end. In the experiments whose results are depicted in Figure 5 and elsewhere as mentioned in the main text, only 25% of the Y seeds were prepared with attachment strands, *i.e.*1 part labeled Y-seeds were mixed with 3 parts unlabeled Y-seeds.

Labeling strand sequences

labeling_strand_ATTO647 /5ATTO647/AAGCGTAGTCGGATCTC
labeling_strand_ATTO488 /5ATTO488N/AAGCGTAGTCGGATCTC

Attachment strand sequences

We use the first 80 attachment strands in Mohammed *et al* [4] from Unused_m13mp18_01 to Unused_m13mp18_80.

2. Methods and protocols

2.1 Self-assembly of nanotube networks

Y-seeded nanotube architectures were grown from Y-shaped DNA origami seeds which first assembled separately. Pre-annealed YSA and YSB were added to the tile solution and were referred to as solution A and solution B respectively. Tiles nucleate on either YSA or YSB to grow nanotubes and after 24 hours of growth, solution A and solution B were mixed at a ratio of 1:1 to create solution C to form networks.

2.1.1 Y-shaped DNA origami seeds (YSA and YSB)

There are two types of hierarchical Y-seeds in this study: YSA and YSB. Both types share the same recipe in Table S6 while using different adapters (sequences are listed in Section 1.2)

Table S6: Recipe of YSA

YSA	Final concentration (nM, if not specified)	Stock concentration (nM, if not specified)	Add (μL)
H_2O			5.05
BSA (mg/mL)	0.05	1	2.50
Y-shaped seed arm A staples	100	3030	1.65

Y-shaped seed arm B staples	100	3030	1.65
Y-shaped seed arm C staples	100	3030	1.65
labeling attachment strand	100	1000	5.00
labeling strand ATTO 488	5000	100,000	2.50
Struts	100	1000	5.00
Adapter strands YSA arm A mix	100	1000	5.00
Adapter strands YSA arm B mix	100	1000	5.00
Adapter strands YSA arm C mix	100	1000	5.00
M13mp18 scaffold	10	100	5.00
10x TAE Mg^{2+} buffer	1 fold	10 folds	5.00
Total			50.00

The recipe for the Y-shaped B seeds is the same as above, only replacing adapter strands of YSA (marked in red) with those for YSB.

BSA: BSA is used to prevent DNA nanostructures from non-specific attachment to Eppendorf tubes, pipette tips, etc.

Arm A/B/C staples mix: Each mixture (A, B or C) containing all 36 staple strands in equal volumes, to a final concentration of staple stocks in water to be 3.03μM each.

Struts mix: The struts are used to connect each pair of arms in the Y-seeds. Mixtures containing all 30 struts strands in water.

Adapters (Y-shaped seed arm A, B, C): Each mixture (arm A, B, or C mix) containing all adapter strands of one arm at a concentration of 1μM in water except the strands with sticky ends [e.g.: For YSA A-arm adapters the sticky ends are: AD1_2REd_armA_2_YSA, AD1_4SEd_armA_2_YSA, AD1_6REd_armA_2_YSA, AD1_8SEd_armA_2_YSA, AD1_10REd_armA_2_YSA, AD1_12SEd_armA_2] which are at 2μM.

Labeling attachment strand: Mixture containing all 80 labeling attachment strands in water at a concentration of 1000nM.

10x TAE Mg^{2+} buffer: Mixture containing 40mM tris-Acetate, 10mM EDTA and 125mM magnesium acetate.

Y-seed annealing protocol [3]:

- Heat to 65˚C for 15 mins.
- Drop the temperature to 47˚C immediately and then incubate at 47˚C for 48h.
- Drop the temperature from 47˚C to room temperature (20˚C) at 1˚C/min.

Y-seeds purification protocol [5]:

We used Amicon Ultra 100 kDa filters to purify the Y-seeds to remove excess staples, adapters, and fluorescent labeling strands.

- Mix 50 µL of unpurified seeds with 350 µL 1x TAE Mg^{2+} buffer in one 0.5 mL filter.
- Centrifuge the filter at 3000g for 4 mins and resuspended the remaining solution with another 350µL 1x TAE Mg^{2+} buffer.
- Repeat step 2 two more times.

After the purification, the Y-seeds can be kept in 4˚C fridge for 1 to 2 weeks.

Y-seeds stock concentration measurement

The concentration was measured by adopting the method developed by Agrawal *et al* [5]. After purification, an imaging solution was prepared by mixing 0.3 µL Y-seed solution with 19.7 µL 1x TAE Mg^{2+} buffer. 6 µL mixture was then transferred to a glass slide to be imaged under a fluorescence microscope with 60x objective. We continued to dilute the purified seeds until 100-200 seeds per field of view (87 µm x 87 µm) were observed, indicating an approximate seed concentration of 6pM in the imaged solution.

2.1.2 Y-seeded nanotube architectures (YNA and YNB) growth

Additional adapter strands were included in the nanotube assembly mixture as we previously found that the presence of additional adapters improved yields of nanotube nucleation from seeds potentially due to attachment of additional adapters to empty adapter binding sites [5].

Table S7: Recipe for Y-seeded nanotube architectures A (YNA) grown from YSA

	Final concentration (nM, if not specified)	Stock concentration (nM, if not specified)	Add (µL)
H_2O			11.8
BSA (mg/mL)	0.05	1	1
REd SEd tiles	50	400	2.5

A arm YSA adapter	4	100	0.8
B arm YSA adapter	4	100	0.8
C arm YSA adapter	4	100	0.8
Seeds A (ATTO 488 labeled)	0.006	0.4	0.3
10x TAE Mg^{2+} buffer	1 fold	10 folds	2
Total			20

Table S8: Recipe for Y-seeded nanotube architectures B (YNB) grown from YSB

	Final concentration (nM, if not specified)	Stock concentration (nM, if not specified)	Add (µL)
H_2O			11.8
BSA (mg/mL)	0.05	1	1
Red SEd tiles	50	400	2.5
A arm YSB adapter	4	100	0.8
B arm YSB adapter	4	100	0.8
C arm YSB adapter	4	100	0.8
YSB (ATTO 488 labeled)	0.006	0.4	0.3
10x TAE Mg^{2+} buffer	1 fold	10 folds	2
Total			20

REd SEd tiles: Mixtures of REd and SEd tiles containing all single strands in water at a stock concentration of 400 nM except the strands with sticky ends which are at 800 nM. The composition of the *Red SEd tiles* mixture means that the strands for each tile except the sticky ends are present at 25 nM while sticky ends are present at 50nM.

Initially, we mixed the above except for YSA or YSB to produce a solution with a volume of 19.7 µL. The solutions were then annealed following the first part of the protocol below. Once the tile mixture reached 45˚C, 0.3µL of pre-annealed YSA or YSB seeds are added to the mixture to a final concentration of 6 pM. The samples were then incubated at 32˚C for at least 15 hours to allow nanotubes to nucleate from Y-seeds and grow.

Annealing protocol:

- Heat to 90˚C
- Drop the temperature from 90˚C to 45˚C at 1˚C/min
- Pause at 45˚C. Quickly add seeds to tile solution
- Drop the temperature from 45˚C to 32˚C at 1˚C/min
- Incubate at 32˚C for around 24 hours

2.1.3 Network formation

A schematic of the network formation process is shown in Figure 2 in the main text. After separately incubating Solutions A and B for about 24 hours, Solutions A and B were mixed in equal volumes in a new tube as Solution C, which was also incubated at 32°C. Solution C was incubated with aliquots being characterized at the times of 1 hour, 4 hours, 8 hours and longer.

2.2 Microscopy and Image Processing

All micrographs were taken using an Olympus IX71 fluorescence microscope with a 60x objective (Olympus NA=1.45, oil immersion) and 1.6x additional magnification. The camera used was an Andor iXon3 Model (No: DU-897E-CS0-#BV). Samples containing Y-shaped DNA origami seeds and Y-seeded nanotube architectures were usually diluted by 10-fold (1μL of sample solution mixed with 9μL of 1x TAE Mg^{2+} buffer) and an aliquot of the diluted solution was applied to glass slides and covered by a coverslip. The dilution was made to ensure that each structure and connection was clear and observable, by preventing different structures from overlapping one another.

Nanotubes were labeled with Cy3 and were imaged using a Cy3 filter cube. YSA and YSB labeled with ATTO 488 were imaged using an ATTO 488 filter cube.

Fluorescence micrographs of Y-seeds were analyzed using the Fiji image J plugin Trackmate to count the number of seeds, when calculating the seed concentration as described in section 2.1.1 before mixing with tiles. The length of each pixel was 170 nm.

3. Additional Data and Analysis

All Python code used in this work is available through GitHub at
https://github.com/yanqijiangjhu/Supplementary-Information-Codes

3.1 Network growth simulation

To understand whether the observed sizes of networks are consistent with a model in which network-size independent end-to-end joining produces networks of a given size, we developed a stochastic kinetic simulation of the joining process. We used the Gillespie method for exact sampling of stochastic kinetics for this simulation. [6, 7, 8]

At time 0, the initial species present were Y-seeded nanotube architectures with one, two or three arms nucleated on either YSA or YSB. 12% (YSA) and 10% (YSB) of the structures were one-armed structures, 42% (YSA) and 36% (YSB) of these structures were two-armed structures, and 46% (YSA) and 54% (YSB) of these were three-armed structures, which were the fraction of structures measured as shown in Figure 3 in the main text. 1000 YSA and 1000 YSB were in the system at time 0. Arms that did not present nanotubes were assumed to be unavailable for joining. Thus, for example, a Y-seeded nanotube architecture with one arm was assumed to have only 1 site available for end-to-end joining.

We assumed that joining reactions were possible between pairs of available ends of complementary type (A-B is complementary, while A-A or B-B are not complementary) and that joining rates were the same for all joining reactions. The microscopic second-order rate constant $k_{joining}$ is used to denote the rate constant of a joining reaction. The joining of ends of complementary types within the same network was not allowed. Simulations were run until no possible joining events remained. 50 identical simulation trajectories (*i.e.* samples) for each $k_{joining}$ were run and their total frequencies were used to plot the data in Fig. 5 in the main text.

The following describes a simple example to illustrate the assumptions of a system containing one YSA and two YSB that each have 2 arms. In this case, there are three potential network candidates, which each has one node (seed). Candidate 1 only has A-type nanotube ends (*i.e.* attachment sites), while candidates 2 and 3 only have B-type nanotube ends. The number of potential joining reactions and the total rates of all the reactions in the system would be calculated by summing the rates of the reactions for each pair of potential reactants.

1. The total joining reaction rate for the reaction between network candidate 1 (the YNA with two arms), and candidate 2 (the first YNB with two arms) is calculated as follows:

$$k_{joining} * (number\ of A\ type\ attachment\ sites\ on\ candidate\ 1) * (number\ of\ B\ type\ attachment\ sites\ on\ candidate\ 2) + k_{joining} * (number\ of\ B\ type\ attachment\ sites\ on\ candidate\ 1) * (number\ of\ A\ type\ attachement\ sites\ on\ candidate\ 2) = ((2 * 2) + (0 * 0))k_{joining} = 4k_{joining}$$

2. The total joining rate for the reaction between network candidate 1 (the YNA with two arms), and network candidate 3 (the second YNB with two arms) is calculated as follows:

$$k_{joining} * (number\ of A\ type\ attachment\ sites\ on\ candidate\ 1) * (number\ of\ B\ type\ attachment\ sites\ on\ candidate\ 3) + k_{joining} * (number\ of\ B\ type\ attachment\ sites\ on\ candidate\ 1) * (number\ of\ A\ type\ attachment\ sites\ on\ candidate\ 3) = ((2 * 2) + (0 * 0))k_{joining} = 4k_{joining}$$

3. The total joining rate for the reaction between network candidate 2 (the first YNB with two arms), and network candidate 3 (the second YNB with two arms) is calculated as follows:

$k_{joining} * (number\ of A\ type\ attachment\ sites\ on\ candidate\ 2)$
$* (number\ of\ B\ type\ attachment\ sites\ on\ candidate\ 3)$
$+\ k_{joining} * (number\ of\ B\ type\ attachment\ sites\ on\ candidate\ 2)$
$* (number\ of\ A\ type\ attachment\ sites\ on\ candidate\ 3) = ((0 * 2) + (2 * 0))k_{joining} = 0$

The total rate of all possible reactions in this system in its current configuration would therefore be $8k_{joining}$.

Simulations were run with $k_{joining,\ sim} = 1\ /s.$ To correctly compare the times from the simulation with the times from experiments, we used a scaling constant q defined as

$$Experiment\ time\ (real\ time) = q * Simulation\ time$$

(Equation 1)

i.e.

$$q = \frac{k_{joinin,\ sim}}{k_{joining}}.$$

To find q, we first computed the volume (V) of the reaction system that was simulated by setting the seed concentrations for the simulation to be the same as in the experiment.

$$[Seed]_{sim} = [Seed]_{real}$$

(Equation 2)

Since the initial concentration of each type of Y-seeded nanotube architecture used in the experiment was 6 pM, and the number of each type of Y-seeds in the simulation was 1000. Equation 2 implies that

$$\frac{1000}{6.022 * 10^{23}} mole * \frac{1}{V\ (L)} = 6.0 * 10^{-12}\ M$$

(Equation 3)

where $6.022 * 10^{23}$ is the Avogadro's number (referred as A in the following). Thus $V = 2.768 * 10^{-10}$ L.

For a bimolecular reaction, the macroscopic rate constant $K_{joining}$ and the microscopic rate constant $k_{joining}$ can be related by the equation:

$$k_{joining} = \frac{K_{joining}}{VA},$$

(Equation 4)

We assumed $K_{joining} = 3.86 * 10^{6}$ /M/s based on the measurements in our previous study [6], so that $k_{joining} = 2.32 * 10^{-8}$ /s .

The scaling factor q is therefore given by

$$q = \frac{k_{joining,\ sim}}{k_{joining}} \frac{1\ /s}{= 2.32 * 10^{-8}/s} = 4.32 * 10^{7}$$

(Equation 5)

3.2 Edge and blob detection

To efficiently measure the sizes of the networks, we developed automated image processing techniques. [9] In the work, we use *edge and blob detection algorithms* to count the number of seeds in a network and the area that the network occupies on the slide, and the related script could be found as *network_metrics.py* in GitHub.

We first processed images from the Cy3 channel to outline the nanotube network. Next, we used blob detection on the corresponding image in the ATTO 488 channel to identify the center of each ATTO 488-labeled Y-seeds. Finally, we combined the network outlines with the information about the seed locations to count the number of seeds in each network.

The detected blobs are bright on dark or dark on bright regions in an image. We used a Laplacian of Gaussian (LoG) function to process the seed channel of each image.
The Laplacian of Gaussian function uses three parameters: *max_sigma*, *num_sigma* and *threshold*.

1) The *max_sigma* refers to the maximum standard deviation for Gaussian Kernel and the higher this value is, the larger the detected blobs are.
2) The *num_sigma* is the number of intermediate values of standard deviations to consider between *min_sigma* and *max_sigma*. The min_sigma is 0.
3) The *threshold* is the absolute lower bound for the scale-space maxima. Reducing this value detects blobs with smaller intensities. It is used to distinguish the detected blobs and the noise.

To include all seeds, we set *max_sigma* to 30 which made it possible to detect larger seed blobs, set *num_sigma* to 10, and *threshold* to 0.01, meaning that local maxima smaller than 0.01 will be ignored. The low threshold value helped detect blobs with lower intensities to prevent false negatives. Below is an example of automated processing of micrographs of tubes and seeds.

After running the script, the user is asked to choose files as input. The tube channel and then the seed channel are chosen. The output will show:

1) Number of detected networks
2) Number of detected seeds in each network
3) The X, Y coordinates of two endpoints of the nanotubes
4) The X, Y coordinates of the seeds

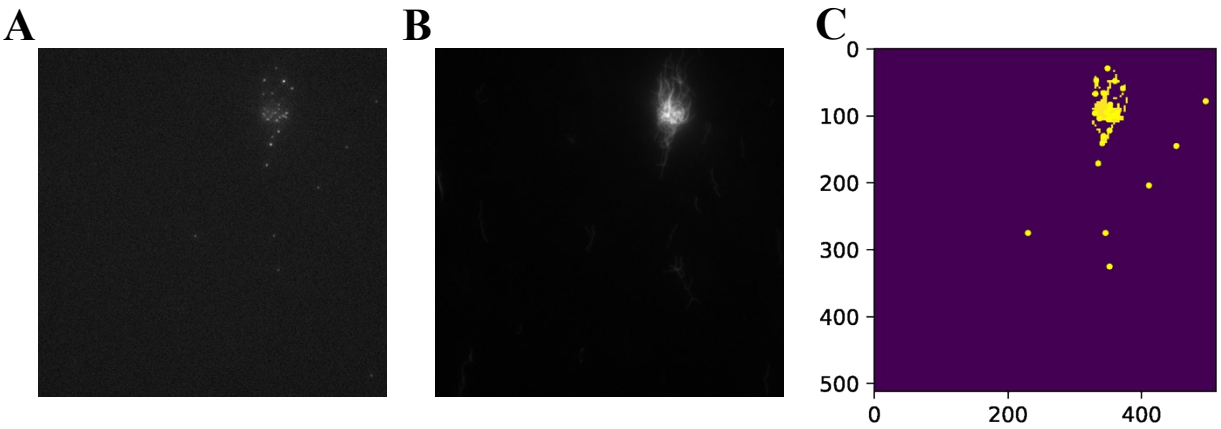

Figure S4: Edge and blob detection on an example image. (A) and (B) are showing the micrographs of the Y seeds and Y-seeded nanotube architectures (two fluorescence channels) taken by an inverted fluorescence microscope (Olympus IX71) after 8 hours of network formation. (C) is the processed image after detecting the seeds and nanotubes using blob and edge detection described above. The yellow dots show where the detected seeds are.

4. Supplementary Figures

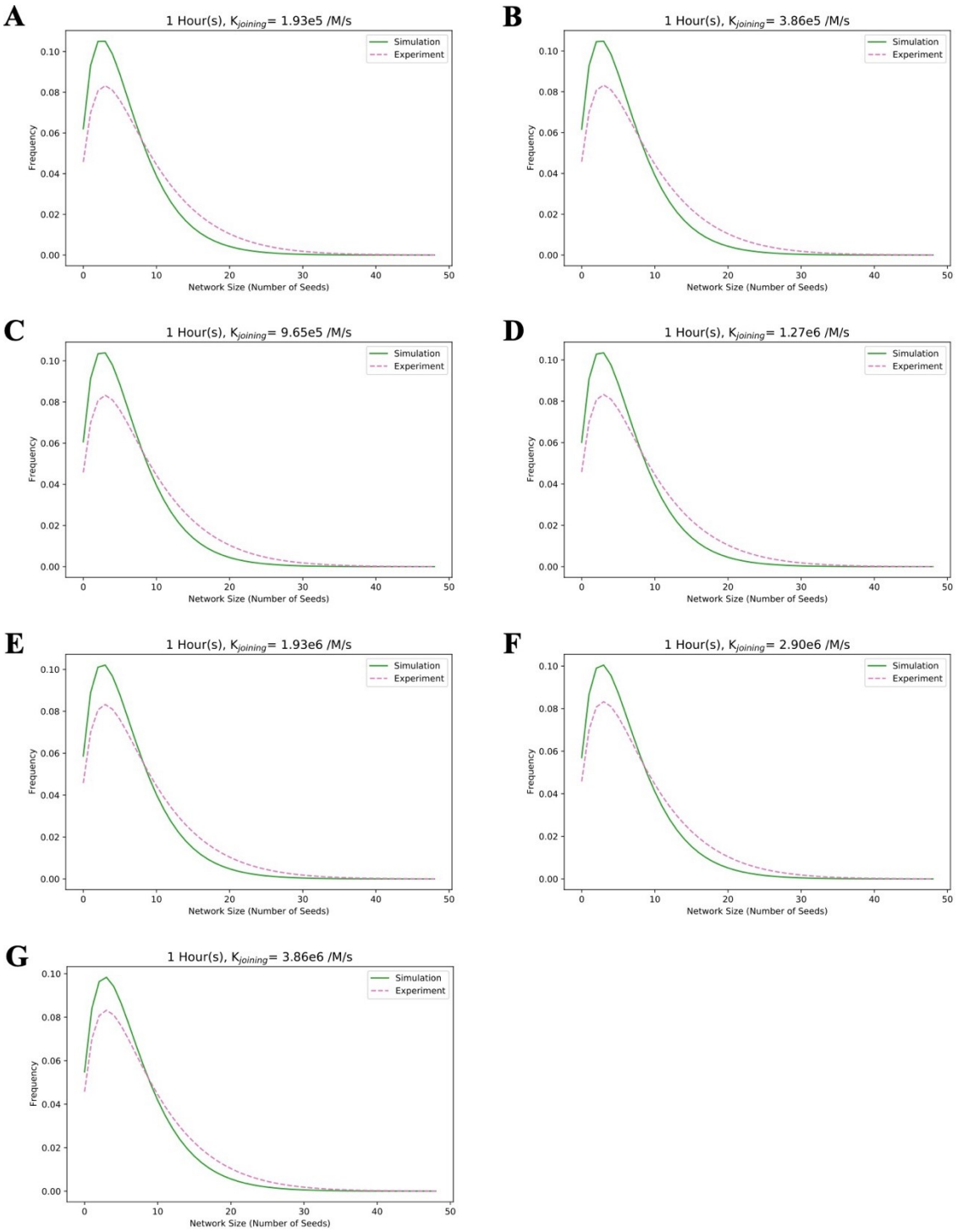

Figure S5: Measurements of network sizes from experiments and predicted by simulations after 1 hour for different joining reaction rate constants. The plots show the individual results included in Figure 6 of the comparison between experiments and simulations using different joining rates. All parameters and conditions are the same as Figure 6.

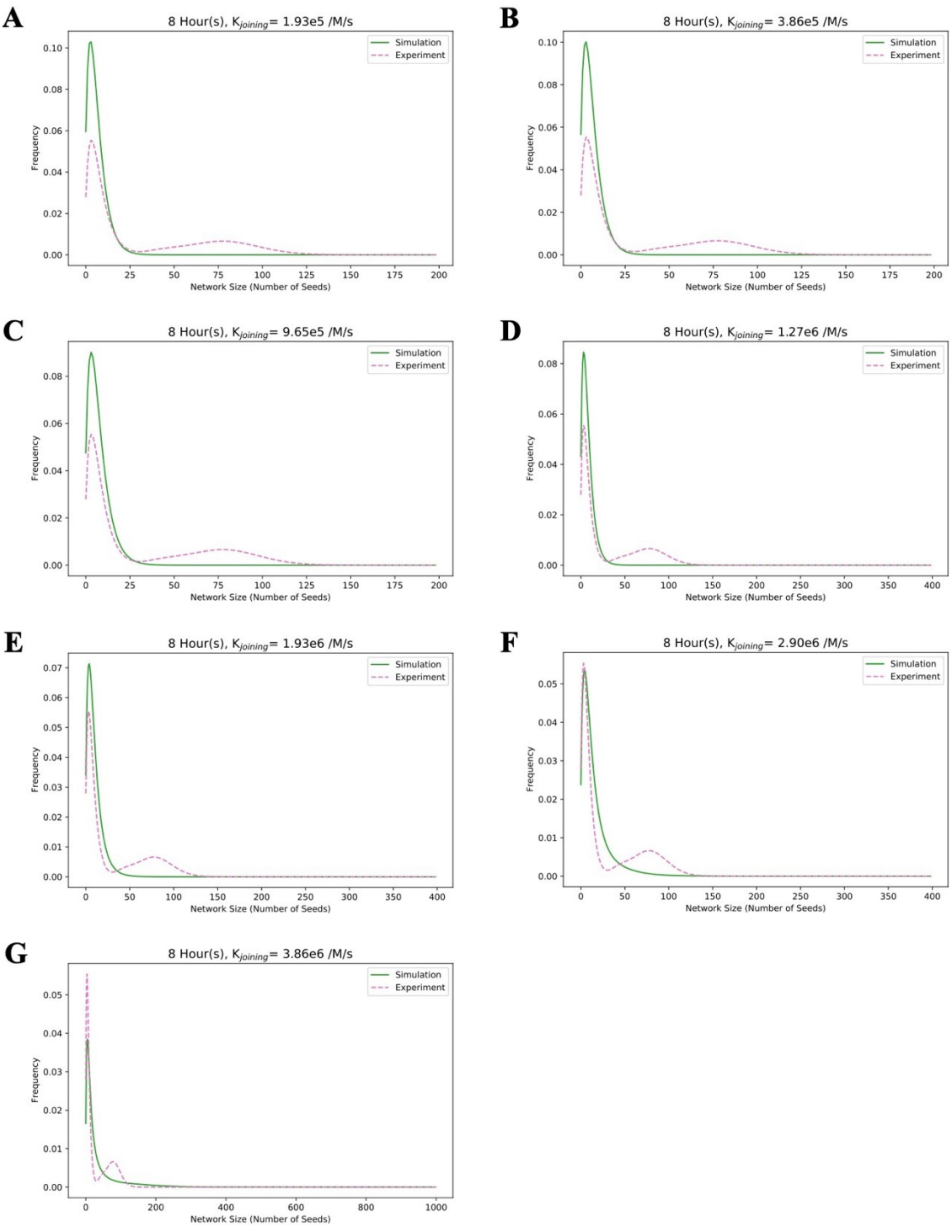

Figure S6: Individual measurement of network size from experiments and predicted by simulation after 8 hours for different joining reaction rate constants. The plots show the individual results included in Figure 6 of the comparison between experiments and simulations using different joining rates to show the performance of each rate. All parameters and conditions are the same as Figure 6.

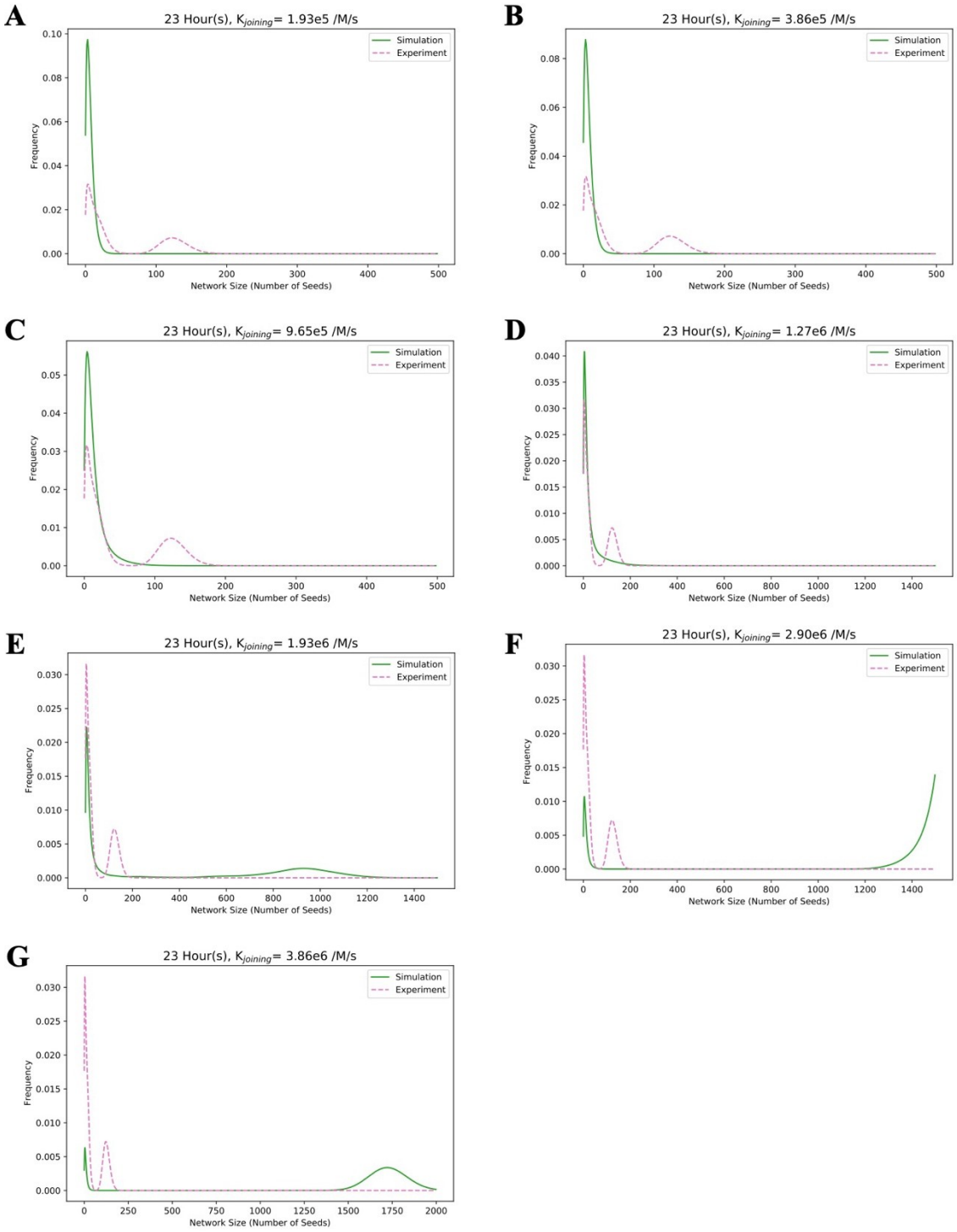

Figure S7: Individual measurement of network size from experiments and predicted by simulation after 23 hours for different joining reaction rate constants. The plots show the individual results included in Figure 6 of the comparison between experiments and simulations using different joining rates to show the performance of each rate. All parameters and conditions are the same as Figure 6.

For the experiments in Figures S5 – S7, we did not expect the model to fit perfectly with the experiments for these largest structures, and the model is assumed to fit better if abundant experimental data are collected. The discrepancy likely results from the fact that, during our imaging, we were not always able to observe the big clusters. In addition, when a big cluster forms, it dominates the process and can result in a large variance – essentially causing large error bars for these data.

References

[1] A. V. Tataurov, Y. You, R. Owczarzy, Biophys. Chem. 2008, 133, 66–70.

[2] P. W. K. Rothemund, A. Ekani-Nkodo, N. Papadakis, A. Kumar, D. K. Fygenson, E. Winfree, J. Am. Chem. Soc. 2004, 126, 16344–16352.

[3] T. D. Jorgenson, A. M. Mohammed, D. K. Agrawal, R. Schulman, ACS Nano 2017, 11, 1927–1936.

[4] A. M. Mohammed, P. Šulc, J. Zenk, R. Schulman, Nat. Nanotechnol. 2017, 12, 312–316.

[5] D. K. Agrawal, R. Jiang, S. Reinhart, A. M. Mohammed, T. D. Jorgenson, R. Schulman, ACS Nano 2017, 11, 9770–9779.

[6] M. S. Pacella, V. Mardanlou, S. Agarwal, A. Patel, E. Jelezniakov, A. M. Mohammed, E. Franco, R. Schulman, Mol. Syst. Des. Eng. 2020, 5, 544–558.

[7] A. Argoti, L. T. Fan, J. Cruz, S. T. Chou, Chem. Eng. Educ. 2008, 42, 35–46.

[8] D. T. Gillespie, J. Phys. Chem. 1977, 81, 2340–2361.

[9] S. Van Der Walt, J. L. Schönberger, J. Nunez-Iglesias, F. Boulogne, J. D. Warner, N. Yager, E. Gouillart, T. Yu, PeerJ 2014, 2014, e453.